

FAINT RADIO SOURCES AND STAR FORMATION HISTORY

Deborah B. Haarsma¹, R. Bruce Partridge¹, Ian Waddington², and
Rogier A. Windhorst²

**For inclusion in the CD-ROM Proceedings of the
19th Texas Symposium on Relativistic Astrophysics,
held December 1998**

(1) *Haverford College*
Haverford, Pennsylvania 19041 USA
Email: dhaarsma@haverford.edu

(2) *Arizona State University*
Department of Physics and Astronomy
Tempe, Arizona 85287-1504 USA

Abstract.

Faint extragalactic radio sources provide important information about the global history of star formation. Sensitive radio observations of the Hubble Deep Field and other fields have found that sub-mJy radio sources are predominantly associated with star formation activity rather than AGN. Radio observations of star forming galaxies have the advantage of being independent of extinction by dust. We use the FIR-radio correlation to compare the radio and FIR backgrounds, and make several conclusions about the star forming galaxies producing the FIR background. We then use the redshift distribution of faint radio sources to determine the evolution of the radio luminosity function, and thus estimate the star formation density as a function of redshift.

1. Introduction

Faint radio sources provide important information about global star formation history. Sensitive radio observations of the Hubble Deep Field (HDF) (Richards *et al* 1998, [1]) and other fields well-studied at optical wavelengths (Windhorst *et al* 1995, [2], Fomalont *et al* 1991, [3]) have shown that sub-mJy radio sources are predominantly associated with star formation activity rather than active galactic nuclei (AGN). The radio luminosity of a galaxy is a reliable predictor of the star formation rate (SFR) for local galaxies (Condon 1992, [4] Cram *et al* 1998, [5]). Estimates of star formation based on radio observations also have the advantage of being independent of extinction by dust, which has caused much difficulty in the determination of star formation history from optical data.

In section 2, we make use of the tight correlation between radio and FIR luminosity for star forming galaxies to compare the FIR and radio backgrounds and to study the sources producing both. In section 3, we determine the evolving radio luminosity function from the observed redshift distribution of faint radio sources, and then

estimate the history of star formation to a redshift of about 3. Throughout, we assume $\Omega_m = 1$, $\Omega_\Lambda = 0$, and $H_0 = 50 \text{ km s}^{-1} \text{ Mpc}^{-1}$. We define the radio spectral index as $S_\nu \propto \nu^{-\alpha}$.

2. FIR vs. Radio Backgrounds

This section follows our recent paper (Haarsma & Partridge 1998, [6]). The far infrared (FIR) background was recently detected with DIRBE (Hauser *et al* 1998, [7]; Dwek *et al* 1998, [8]), and is most likely the collective emission of star forming galaxies. We use the radio-FIR correlation for individual galaxies (Helou, Soifer, & Rowan-Robinson 1985, [9]) to calculate the radio background associated with the FIR background, assuming that the bulk of emission is from $z \sim 1$. We find the radio background associated with the FIR background has a brightness temperature of $T_{40 \text{ cm}} = 0.31 \text{ K}$, or $T_{170 \text{ cm}} \sim 15 \text{ K}$ (scaled using a spectral index of $\alpha = 0.7$). At 170 cm (178 MHz), the observed radio background is $T_{170 \text{ cm}} = 30 \pm 7 \text{ K}$ (Bridle 1967, [10]). This allows us to draw several conclusions about the faint sources making up the FIR background:

- (i) The radio emission from these sources makes up about half of the observed extragalactic radio background. (The other half is the summed radio emission of AGN.)
- (ii) Since (i) is in agreement with other radio observations (Condon 1989, [11]), the FIR-radio correlation appears to hold even for the very faint sources making up the FIR background. This confirms the assumption that the FIR background between about 140 and 240 μm is dominated by star-formation, not AGN activity.
- (iii) By quantitatively comparing the radio and FIR backgrounds, we find a relationship for the sources contributing to the background,

$$A \left(\frac{1+z}{8.5} \right)^\alpha = 0.20 \pm 0.05, \quad (1)$$

where α is their radio spectral index, A is the fraction of the radio background they produce (from (i), $A \sim 0.5$), and z is their mean redshift. This function is plotted in Figure 1. Note that the redshift z is the mean redshift of the sources dominating the FIR and radio backgrounds, which is not necessarily the redshift of peak star formation activity (see §3).

- (iv) By extrapolating the 3.6 cm $\log N - \log S$ curve to fainter flux densities, we estimate that most of the FIR background is produced by sources whose 3.6 cm flux density is greater than about $1 \mu\text{Jy}$. This lower limit is consistent with other work (Windhorst *et al* 1993, [12]), but has more interesting observational consequences. An RMS sensitivity of $1.5 \mu\text{Jy}$ has already been reached in VLA observations (Partridge *et al* 1997, [13]). The $\log N - \log S$ curve indicates that the number density of $S \geq 1 \mu\text{Jy}$ sources is about $25/\text{arcmin}^2$, similar to some model predictions (Guideroni *et al* 1998, [14]). At this density, these sources will cause SIRTf to encounter confusion problems at 160 μm .

3. Radio Star Formation History

In this section, we use the redshift distribution of faint radio sources to determine the evolution of the radio luminosity function, and the evolution of the star formation rate density.

3.1. Data

Three fields have been observed to microJy sensitivity at centimeter wavelengths and also have extensive photometric and spectroscopic data: the Hubble Deep Field (HDF), the Medium Deep Survey (MDS), and the V15 field. Table 1 gives the details of the three fields and references. For the first time we have a sample of microJy radio sources with nearly complete optical identifications and about 50% complete redshift measurements. We assume that all sources detected at these flux levels are star-forming galaxies, since optical identifications indicate that $\sim 80\%$ of these radio sources have spiral or irregular counterparts (Richards *et al* 1998, [1]). The known quasars (two in the MDS sample, none in the HDF or V15 samples) were removed. In the flanking fields of the HDF, we have used the relationship between redshift and K-band magnitude (Lilly, Longair, & Allington-Smith 1985, [15]) to estimate redshifts for 10 sources without spectroscopic values. For the remaining sources without redshifts, we arbitrarily selected redshifts to fill in gaps in the redshift distribution, in order to illustrate the total number of sources that will ultimately appear on the plot. Photometric redshifts for these sources are currently being calculated (Waddington & Windhorst, in preparation), and will be included in future work.

To compare these data to the model, we calculate $n(z)$, the average number of sources per arcmin² in each redshift bin. This requires a correction for the varying sensitivity across the primary beam of the radio observations (Katgert, Oort, & Windhorst 1988, [16]; Martin, Partridge, & Rood 1980, [17]). For example, a faint source which could only be detected at the center of the field contributes more to $n(z)$ than a strong source which could be detected over the entire primary beam area. The resulting redshift distributions are plotted in Figures 4 and 8.

It is interesting how different the MDS and HDF distributions are, even though the surveys were both performed at 8 GHz with similar flux limits. The average source density (including all sources) is 1.26 sources/arcmin² in the HDF, but 2.63 sources/arcmin² in the MDS field (the V15 field at 5 GHz has 0.736 sources/arcmin²). The density of sources in the MDS field is over twice that of the HDF field, possibly due to galaxy clustering. In the analysis below, we fit the model to the data in all three fields simultaneously.

3.2. Calculations

In order to determine the star formation history, we must first determine the evolving radio luminosity function. We used two versions of the local 1.4 GHz luminosity function for star-forming/spiral galaxies. We define the luminosity function $\phi(L_{e,1.4})$ as the number per comoving Mpc³ per $d\log_{10} L$ of star-forming radio sources with emitted luminosity $L_{e,1.4}$ (W/Hz) at 1.4 GHz. Condon (1989, [11]) uses the following form for the luminosity function (but different notation),

$$\log_{10}[\phi(L_{e,1.4})]d\log_{10} L = 28.43 + Y - 1.5 \log_{10} L_{e,1.4}$$

Field	Location	Band	Flux limit	N	N _z	Reference
Hubble Deep Field	12h+62d	8 GHz	9 μJy	29	13 (+10)	[1]
Medium Deep Survey	13h+42d	8 GHz	8.8 μJy	19	10	[2]
V15 field	14h+52d	5 GHz	16 μJy	35	18	[3, 27]

Table 1. Summary of three deep radio surveys. The flux limit of the complete catalog for each field is approximately 5 times the RMS noise of the observation, but varies across the field. N is the total number of sources above the flux limit, and N_z is the number of those sources with spectroscopic redshifts. An additional 10 redshifts were estimated in the HDF from their K-band magnitudes.

$$- \left[B^2 + \frac{1}{W^2} (\log_{10} L_{e,1.4} - X)^2 \right]^{1/2} d \log_{10} L, \quad (2)$$

with the fitted parameters for star-forming galaxies of $Y = 2.88$, $X = 22.40$, $W = 2/3$, and $B = 1.5$. Serjeant *et al* (1998, [18]) use the standard Schechter form,

$$\phi(L_{e,1.4}) d \log_{10} L = \phi_* \ln 10 \left(\frac{L_{e,1.4}}{L_*} \right)^{(1+\alpha_l)} \exp \left(-\frac{L_{e,1.4}}{L_*} \right) d \log_{10} L \quad (3)$$

where a factor of $L \ln 10$ has been included to convert the function from dL to $d \log_{10} L$. Serjeant *et al* find fitted parameters of $\phi_* = 4.9 \times 10^{-4} \text{ Mpc}^{-3}$, $L_* = 2.8 \times 10^{22} \text{ W/Hz}$, and $\alpha_l = -1.29$.

To describe the evolution of the luminosity function, we use the functional form suggested by Condon (1984a, [19], eq. 24), a power-law in $(1+z)$ with an exponential cut-off at high redshift. The luminosity evolves as

$$f(z) = (1+z)^Q \exp \left[-\left(\frac{z}{z_q} \right)^q \right], \quad (4)$$

and the number density evolves as

$$g(z) = (1+z)^P \exp \left[-\left(\frac{z}{z_p} \right)^p \right]. \quad (5)$$

This gives six parameters $\{Q, q, z_q, P, p, z_p\}$ to use in describing the evolution. When fitting for the parameters, we constrained the functions $g(z)$ and $f(z)$ to the physically reasonable ranges of $1 < g(z) < 100$, $1 < f(z) < 100$ for $0 < z < 3$. The general expression for the evolving luminosity function is then (Condon 1984b, [20])

$$\phi(L_{e,1.4}, z) = g(z) \phi \left(\frac{L_{e,1.4}}{f(z)}, 0 \right). \quad (6)$$

To use this expression at an arbitrary observing frequency ν and redshift z , we must convert the observed luminosity $L_{o,\nu}$ to 1.4 GHz and do the K-correction, i.e.

$$L_{e,1.4} = L_{o,\nu} \left(\frac{\nu}{1.4 \text{ GHz}} \right)^\alpha (1+z)^\alpha \quad (7)$$

where α is the radio spectral index, as defined in §1. We have assumed $\alpha = 0.4$ for all calculations in §3 (Windhorst *et al* 1993, [12]).

The evolving luminosity function can be used to predict the observed redshift distribution. The number of sources per redshift bin Δz that could be detected in a survey of angular area $\Delta\Omega$ and flux limit S_{lim} at frequency ν is

$$n(z) = V_c(z, \Delta z, \Delta\Omega) \int_{L'(z)}^{\text{inf}} \phi(L_{e,1.4}, z) d \log_{10} L \quad (8)$$

where the lower limit of the integral is

$$L'(z) = 9.5 \times 10^{12} \frac{\text{W}}{\text{Hz}} \left(\frac{S_{lim}}{\mu\text{Jy}} \right) (1+z)^\alpha \left(\frac{\nu}{1.4 \text{ GHz}} \right)^\alpha 4\pi \left(\frac{D_L(z)}{\text{Mpc}} \right)^2 \quad (9)$$

and D_L is the luminosity distance. The comoving volume in a shell from z to $z + \Delta z$ and angular size $\Delta\Omega$ is

$$\begin{aligned} V_c(z, \Delta z, \Delta\Omega) &= \int d\Omega \int r^2(z) dr \\ &= \frac{\Delta\Omega}{\text{ster}} \left(\frac{\text{ster}}{1.18 \times 10^7 \text{ arcmin}^2} \right) \frac{[r^3(z + \Delta z) - r^3(z)]}{3} \end{aligned} \quad (10)$$

where the comoving distance is

$$r(z) = \frac{2c}{H_0} \left(1 - \frac{1}{\sqrt{1+z}} \right) \quad (11)$$

for our assumed cosmology (see §1). We have used $\Delta\Omega = 1 \text{ arcmin}^2$ for comparison to the data in Figures 4 and 8.

The evolving luminosity function also allows us to calculate the star formation history. For an individual galaxy, the star formation rate is directly proportional to its radio luminosity (Condon 1992, [4]):

$$\text{SFR} = Q \left(\frac{L_\nu / \frac{\text{W}}{\text{Hz}}}{5.3 \times 10^{21} \left(\frac{\nu}{\text{GHz}} \right)^{-0.8} + 5.5 \times 10^{20} \left(\frac{\nu}{\text{GHz}} \right)^{-0.1}} \right) \frac{M_\odot}{\text{yr}} \quad (12)$$

The radio luminosity is primarily due to synchrotron emission from supernova remnants (the first term in the denominator) plus a small thermal component (the second term). Both components are proportional to the formation rate of high-mass stars which produce supernova ($M > 5M_\odot$), so the factor Q is included to account for the mass of all stars ($0.1 - 100M_\odot$),

$$Q = \frac{\int_{0.1M_\odot}^{100M_\odot} M\psi(M)dM}{\int_{5M_\odot}^{100M_\odot} M\psi(M)dM}, \quad (13)$$

where $\psi(M) \propto M^{-x}$ is the initial mass function (IMF). We have assumed throughout a Salpeter IMF ($x = 2.35$), for which $Q = 5.5$. If an upper limit of $125M_\odot$ is used, then $Q = 5.9$.

In order to use eq. 12 at high redshift, both L_ν and ν in the equation must be K-corrected to the emitted luminosity at the emission frequency. Are there other ways in which this relation evolves? The thermal term is much smaller than the synchrotron term, so evolution in the thermal term will have little effect. In the synchrotron term, the dependence on the supernova environment is weak. One component that might cause significant evolution in eq. 12 is an evolving IMF, entering through the factor Q .

In active starbursts, the IMF may be weighted to high-mass stars (Elmegreen 1998, [21]), which would result in a smaller value of Q . However, the smallest Q is unity (when virtually all mass occurs in high-mass stars), so the strongest decrease due to IMF evolution would be roughly a factor of five.

To determine the star formation rate per comoving volume, we simply substitute the radio luminosity density for L_ν in eq. 12. The star formation rate depends on the emitted (rather than observed) luminosity density. The luminosity density emitted at 1.4 GHz can be easily found from the evolving luminosity function,

$$\rho_{e,1.4}(z) = \int_{-\text{inf}}^{\text{inf}} L_{e,1.4} \phi(L_{e,1.4}, z) d \log_{10} L. \quad (14)$$

Thus the predicted star formation history is

$$\psi(z) = Q \left(\frac{\rho_{e,1.4}(z)}{4.6 \times 10^{21} \frac{\text{W}}{\text{HzMpc}^3}} \right) \frac{M_\odot}{\text{yrMpc}^3} \quad (15)$$

where 1.4 GHz is used in the denominator of eq. 12 (no K-correction is needed because the luminosity density is the emitted value).

3.3. Results

We use the formulation of §3.2 to determine the star formation history from the evolving luminosity function. To determine the evolution parameters, we compare the model to the observed $n(z)$ for the three surveys. We immediately found that pure luminosity evolution [$f(z) = (1+z)^3$ and $g(z) = 1$], as often suggested in the literature, is a poor fit for the faint star-forming galaxy population (the predicted $n(z)$ is too small and has a very long high-redshift tail). The model fit of Condon (1984a, [19]), $\{Q = 3.5, P = 1.75, p = 1.8, z_p = 1\}$ with no exponential cut off in luminosity evolution, is much better (more reasonable redshift dependence, but $n(z)$ is still too low). To improve on these models, we adjust the evolution parameters $\{Q, q, z_q, P, p, z_p\}$ to improve the model fit to the $n(z)$ data, using a downhill simplex algorithm (Press *et al* 1992, [22]) to find the global χ^2 minimum. We performed this fit using both the Condon (1989, [11]) luminosity function (Model C, see eq. 2) and the Serjeant *et al* (1998, [18]) luminosity function (Model S, see eq. 3).

In Model C we use the luminosity function of Condon (1989, [11]). The fitted evolution parameters were $\{Q = 7.6, q = 1.3, z_q = 0.48, P = 1.6, p = 1.2, z_p = 1.8\}$. The resulting evolution factors $f(z)$ and $g(z)$ are plotted in Figure 2 and the resulting luminosity function is shown in Figure 3. Although the term $(1+z)^{7.6}$ seems extreme, when combined with the exponential cut-off the luminosity evolution $f(z)$ is reasonable. The fit to the the redshift distribution is shown in Figure 4. The fit significantly underestimates the total number of sources in the MDS field, but only slightly underestimates the other two fields. The V15 survey has the largest total number of sources and thus has the most weight during fitting, so the result is a better fit for V15 than the other fields. Finally, Figure 5 shows our predicted star formation history (heavy line) along with model predictions from several others (thin lines). The vertical lines indicate the $1/\sqrt{N}$ uncertainty, where N is the sum of galaxies at that redshift from the three surveys. The Model C prediction is in good agreement with other models at low redshift (the curve follows closely the prediction of Pei & Fall 1995, [23], as plotted in Dwek *et al* 1998, [8], figure 3), which is impressive given that

no free parameters were adjusted to fit the $z = 0$ value. The predicted star formation history peaks around a redshift of 1, and falls off more quickly than other models at high redshift.

In Model S we use the luminosity function of Serjeant *et al* (1998, [18]) (see eq. 3 above). The fitted evolution parameters were $\{Q = 4.3, q = 2.1, z_q = 1.3, P = 1.3, p = 1.7, z_p = 2.3\}$. The resulting evolution factors $f(z)$ and $g(z)$ are plotted in Figure 6 and the resulting luminosity function is shown in Figure 7. Despite very different individual parameters ($Q = 4.3$ vs. $Q = 7.6$), the two fits have similar functions $f(z)$ and $g(z)$. The predicted redshift distribution (Figure 8) is peaked at a slightly lower redshift and has a slightly longer tail than Model C. The predicted star formation history (Figure 9) has a larger local value than Model C, but still less than that predicted by Baugh *et al* (1998, [24]) (thin solid line). The peak is around a redshift of 1.4, and falls off less rapidly than Model C at high redshift.

3.4. Discussion

The star formation histories predicted by Model C and Model S both fall off more quickly at high redshift than model predictions by others. However, we are considering several refinements to our model that might modify this result. We are currently determining additional photometric redshifts (Waddington & Windhorst, in preparation), which will make the modeling more reliable particularly at high redshift. The predicted shape of the star formation history is limited by the functional form we chose for evolution (eq. 4 and 5), and we plan to experiment with other functions. If the IMF is evolving, or is dependent on environment, this would also affect our results. The relationship between star formation rate and radio luminosity (eq. 12) might be evolving in addition to its dependence on an evolving IMF. Finally, we have not explored the dependence of our results on cosmological parameters.

This method has the potential to be an important indicator of star formation history. Radio luminosity is a reliable indicator of star formation rate in local galaxies, and is not affected by dust extinction. While others are performing similar calculations (Cram *et al* 1998, [5]; Cram 1998, [25]; Mobasher *et al* 1999, [26], Serjeant *et al* 1998, [18]), the survey data used here are complete to a substantially lower flux limit, with nearly complete knowledge of optical counterparts and $\sim 50\%$ completeness in redshifts. This allows us to place stronger constraints on the evolving radio luminosity function and to probe star formation activity to much higher redshifts.

Acknowledgments

We are grateful to Eric Richards for helpful discussions. D.H. thanks the National Science Foundation for travel support for this Symposium. D.H. and B.P. acknowledge the support of NSF AST 96-16971.

References

- [1] Richards, E. A., Kellermann, K. I., Fomalont, E. B., Windhorst, R. A., & Partridge, R. B. 1998, *AJ*, 116, 1039
- [2] Windhorst, R. A., Fomalont, E. B., Kellermann, K. I., Partridge, R. B., Richards, E., Franklin, B. E., Pascarella, S. M., & Griffiths, R. E. 1995, *Nature*, 375, 471
- [3] Fomalont, E. B., Kellermann, K. I., Windhorst, R. A., & Kristian, J. A. 1991, *AJ*, 102, 1258
- [4] Condon, J. J. 1992, *ARA&A*, 30, 575

- [5] Cram, L., Hopkins, A., Mobasher, B., & Rowan-Robinson, M. 1998, ApJ, 507, 155
- [6] Haarsma, D. B., & Partridge, R. B. 1998, ApJ, 503, L5
- [7] Hauser, M. G., et al. 1998, ApJ, 508, 25
- [8] Dwek, E., et al. 1998, ApJ, 508, 106
- [9] Helou, G., Soifer, B. T., & Rowan-Robinson, M. 1985, ApJ, 298, L7
- [10] Bridle, A. H. 1967, MNRAS, 136, 219
- [11] Condon, J. J. 1989, ApJ, 338, 13
- [12] Windhorst, R. A., Fomalont, E. B., Partridge, R. B., & Lowenthal, J. D. 1993, ApJ, 405, 498
- [13] Partridge, R. B., Richards, E. A., Fomalont, E. B., Kellermann, K. I., & Windhorst, R. A. 1997, ApJ, 483, 38
- [14] Guiderdoni, B., Hivon, E., Bouchet, F. R., & Maffei, B. 1998, MNRAS, 295, 877
- [15] Lilly, S. J., Longair, M. S., & Allington-Smith, J. R. 1985, MNRAS, 215, 37
- [16] Katgert, P., Oort, M. J. A., & Windhorst, R. A. 1988, A&A, 195, 21
- [17] Martin, H. M., Partridge, R. B., and Rood, R. T. 1980, ApJ, 240, L79
- [18] Serjeant, S., Gruppioni, C., & Oliver, S. 1998, preprint astro-ph/9808259
- [19] Condon, J. J. 1984a, ApJ, 284, 44
- [20] Condon, J. J. 1984b, ApJ, 287, 461
- [21] Elmegreen, B. G. 1998, in Unsolved Problems in Stellar Evolution, ed. M. Livio (Cambridge: Cambridge University Press)
- [22] Press, W. H., Flannery, B. P., Teukolsky, S. A., & Vetterling, W. T. 1992, Numerical Recipes (2nd ed.) (Cambridge University Press)
- [23] Pei, Y. C., & Fall, S. M. 1995, ApJ, 454, 69
- [24] Baugh, C. M., Cole, S., Frenk, C. S., & Lacey, C. G. 1998, ApJ, 498, 504
- [25] Cram, L. 1998, ApJ, 506, L85
- [26] Mobasher, B., Cram, L., Georgakakis, A., & Hopkins, A. 1999
- [27] Hammer, F., Crampton, D., Lilly, S. J., LeFevre, O., & Kenet, T. 1995, MNRAS, 276, 1085
- [28] Guiderdoni, B., Bouchet, F. R., Devriendt, J., Hivon, E., & Puget, J. L. 1999, preprint astro-ph/9902141

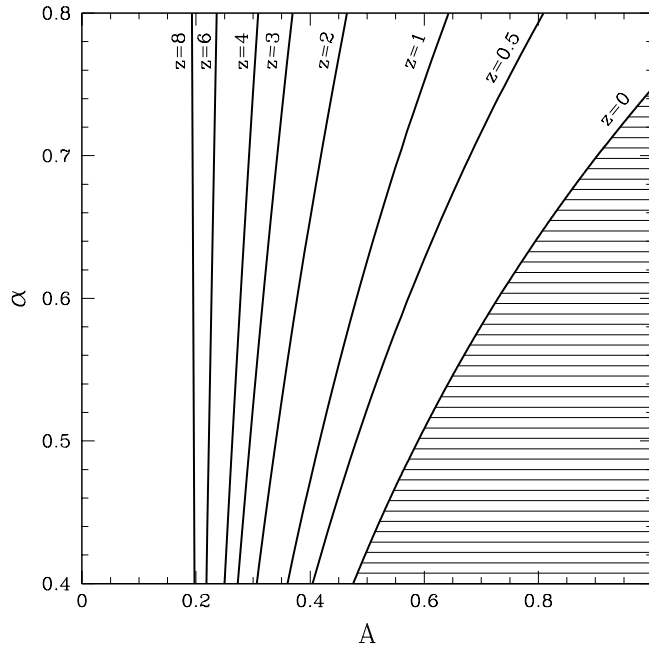


Figure 1. Relationship between the radio spectral index α , the ratio of star-formation flux to the total radio background A , and the typical redshift z for the sources making up the FIR background.

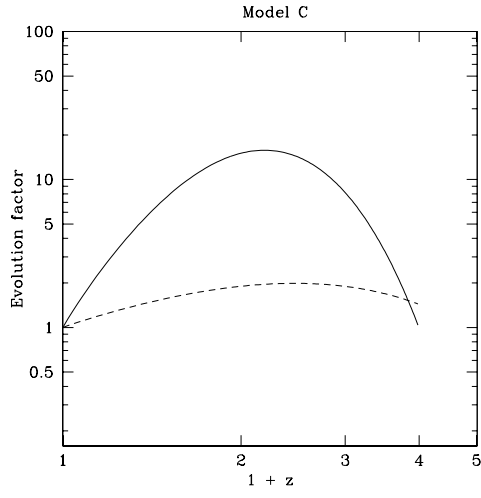


Figure 2. Evolution functions for Model C. The solid line is $f(z)$ (luminosity evolution), and the dashed line is $g(z)$ (number density evolution).

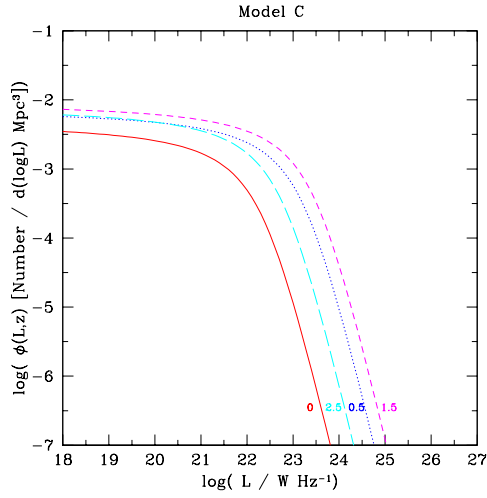


Figure 3. Evolving luminosity function for Model C. The labels indicate the redshift for each curve, for $z = 0, 0.5, 1.5,$ and 2.5 .

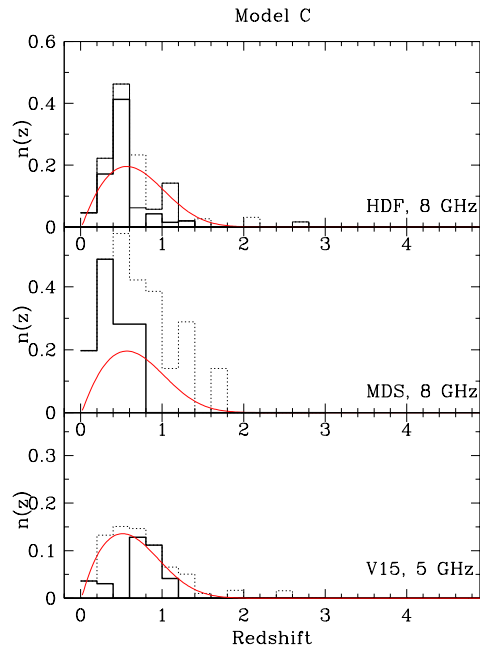


Figure 4. Redshift distribution $n(z)$, number per arcmin² per redshift bin. The curve shows the prediction of Model C. The data histograms indicate spectroscopic redshifts [heavy line], spectroscopic redshifts plus estimates from K magnitudes [thin line histogram], and all sources (including arbitrary redshifts for remaining sources) [dotted line].

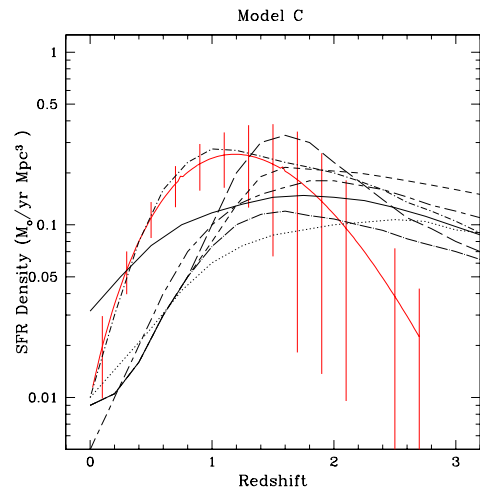


Figure 5. Star formation history. The heavy curve is the prediction of Model C, with vertical lines indicating the uncertainty. The remaining lines indicate star formation histories predicted by several other models: solid line (Baugh *et al* 1998, [22]), dotted line (Guiderdoni *et al* 1999 [26]), other broken lines (Dwek *et al* 1998, [8], figure 3).

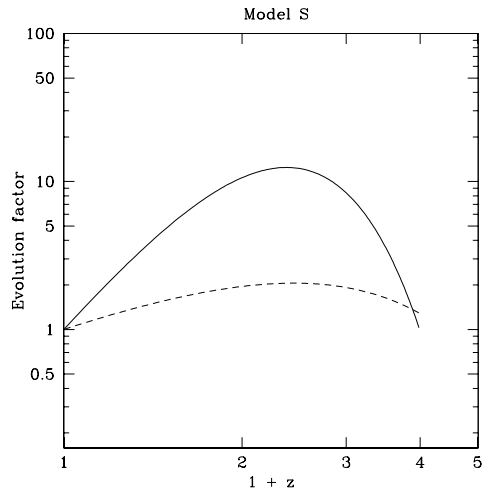


Figure 6. Evolution functions for Model S. The solid line is $f(z)$ (luminosity evolution), and the dashed line is $g(z)$ (number density evolution).

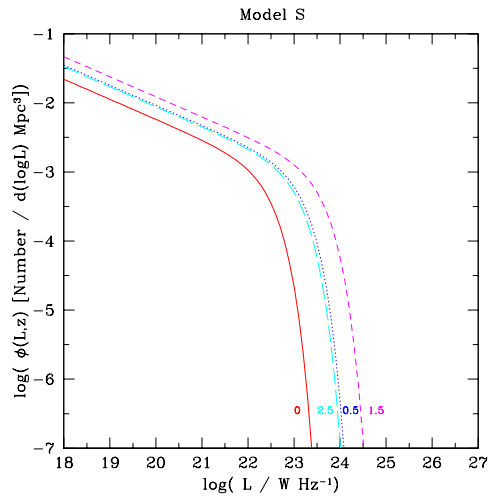


Figure 7. Evolving luminosity function for Model S. The labels indicate the redshift for each curve, for $z = 0, 0.5, 1.5,$ and 2.5 .

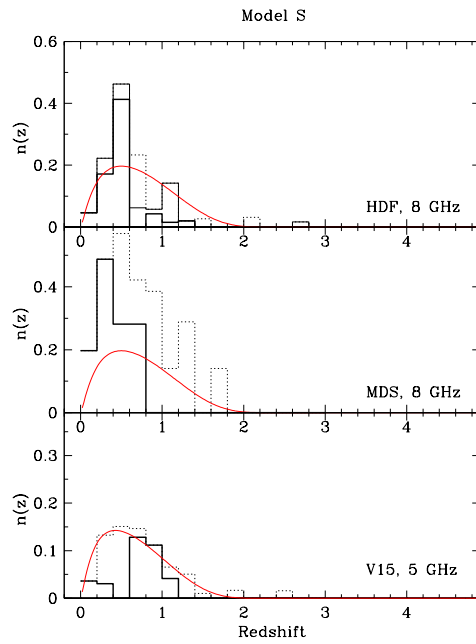


Figure 8. Redshift distribution $n(z)$, number per arcmin² per redshift bin. The curve shows the prediction of Model S. The data histograms indicate spectroscopic redshifts [heavy line], spectroscopic redshifts plus estimates from K magnitudes [thin line histogram], and all sources (including arbitrary redshifts for remaining sources) [dotted line].

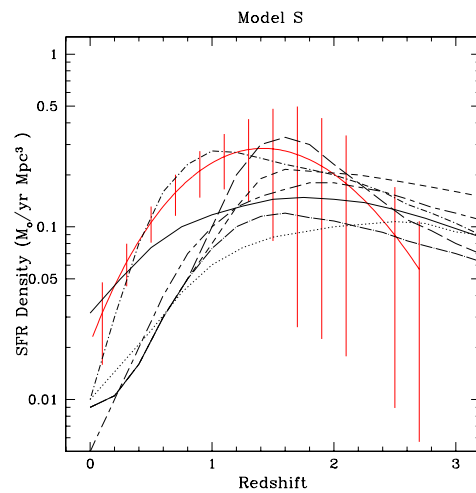


Figure 9. Star formation history. The heavy curve is the prediction of Model S, with vertical lines indicating the uncertainty. The remaining lines indicate star formation histories predicted by several other models: solid line (Baugh *et al* 1998, [22]), dotted line (Guideroni *et al* 1999, [26]), other broken lines (Dwek *et al* 1998, [8], figure 3).